DEM generation from SPOT-5 3-fold along track stereoscopic imagery using autocalibration

W. Kornus *, R. Alamús, A. Ruiz, J. Talaya

Institut Cartogràfic de Catalunya (ICC), Parc de Montjuïc, 08038 Barcelona, Spain

Abstract

This paper describes the derivation and accuracy assessment of Digital Elevation Models (DEM) from 3-fold along-track stereoscopic SPOT-5 imagery. The work was conducted in the scope of the HRS (Haute Résolution Stéréoscopique)-Scientific Assessment Program, organized by the Centre National d'Études Spatiales (CNES) and the International Society of Photogrammetry and Remote Sensing (ISPRS). The orientation of the SPOT-5 image scene is reconstructed by bundle adjustment using ground control points. The functional model is based on correction polynomials and permits autocalibration. At 17 independent check points a RMS-error of 2 m was achieved. DEM are produced in two different ways: The more rigorous way employs an automatic region growing image matching process generating a dense point cloud in image space, transforms it into the object space using the estimated model parameters and converts it into a regular grid DEM. In a second approach the commercial software ISAE and rational functions are applied. The comparison with a digital terrain model (DTM) of superior accuracy yields standard deviations better than 5 m in flat and moderate terrain and better than 10 m in mountainous regions. With ISAE a DEM for the entire image area (approx. 60×80 km) is produced with a standard deviation of approximately 8 m. All grid points were generated fully automatically, i.e. the presented standard deviations still include the effect of large differences between the produced DEM and the DTM.

1. Introduction

The presented work is part of the HRS study (Baudoin et al., 2004), where the ICC participated as principal investigator. The goal of the study was to produce a DEM from the given SPOT-5 data and to assess the derived DEM quality and accuracy. SPOT-5 is the first satellite of the SPOT family with along-track stereo imaging capability. The two HRS (Haute Résolution Stéréoscopique) cameras HRS1 and HRS2 are tilted by ±20° and acquire nearly simultaneous stereo-pairs (at a 90-s interval) of 120 km swath, along the track of the satellite, with a B/H ratio of 0.8. A continuous strip of 600 km length is covered stereoscopically with ground sampling distance (GSD) of 10 m across track and 5 m along. The nadir looking panchromatic HRG (Haute Résolution Géométrique) instrument provides imagery at 5 m GSD in the monospectral bands HMA and HMB, at 10 m in the multi-

---

* Corresponding author. Tel.: +34 93 567 1500; fax: +34 93 567 1567.

 E-mail addresses: wkornus@icc.es (W. Kornus), ralamus@icc.es (R. Alamús), toni@icc.es (A. Ruiz), talaya@icc.es (J. Talaya).

spectral bands XS1, XS2, XS3 and at 20 m GSD in SWIR. The ground pixel of HMA and HMB scenes are interleaved and shifted 2.5 m to enable the interpolation of so-called THR (French acronym for 'very high resolution') images (SPOT Magazine, 2000). The size of an image scene is 12,000×12,000 pixel (24,000×24,000 pixel in case of the THR image). A summary of the SPOT-5 payload and mission characteristics is given in (Bouillon et al., 2006-this issue).

2. Initial data

The scene covering the Barcelona area was selected from the nine HRS study test areas. The data set provided by CNES comprised 5 images (HRS1, HRS2, HMA, HMB and THR) and auxiliary data (time series of orbit positions, velocities and attitude angles, look angles for each CCD element, etc.). In this study the images HRS1 and HRS2 of the HRS instrument and the THR image of the HRG instrument are used, in the following simplistically referred as HRS- and HRG-images. The ICC provided the

reference data set consisting of a regular DTM of 15 m grid step size and 1.1 m accuracy (1 σ) covering the total area of the images and 32 orthoimages of 0.5 m pixel size and 0.5 m accuracy (1 σ) for 8 test sites of approximately 10×14 km (see Fig. 1). Fig. 2 shows the radiometrically improved HRG image and the HRS1 image with the different resolution in scan and flight direction.

3. Data evaluation

The applied work flow as well as the structure of this paper is subdivided into 7 steps:

1. Direct geo-referencing of the images using the supplied orientation parameters (auxiliary data)
2. Measurement of control and check points in the 8 test sites
3. Mass point generation in image space using region growing matching algorithm.
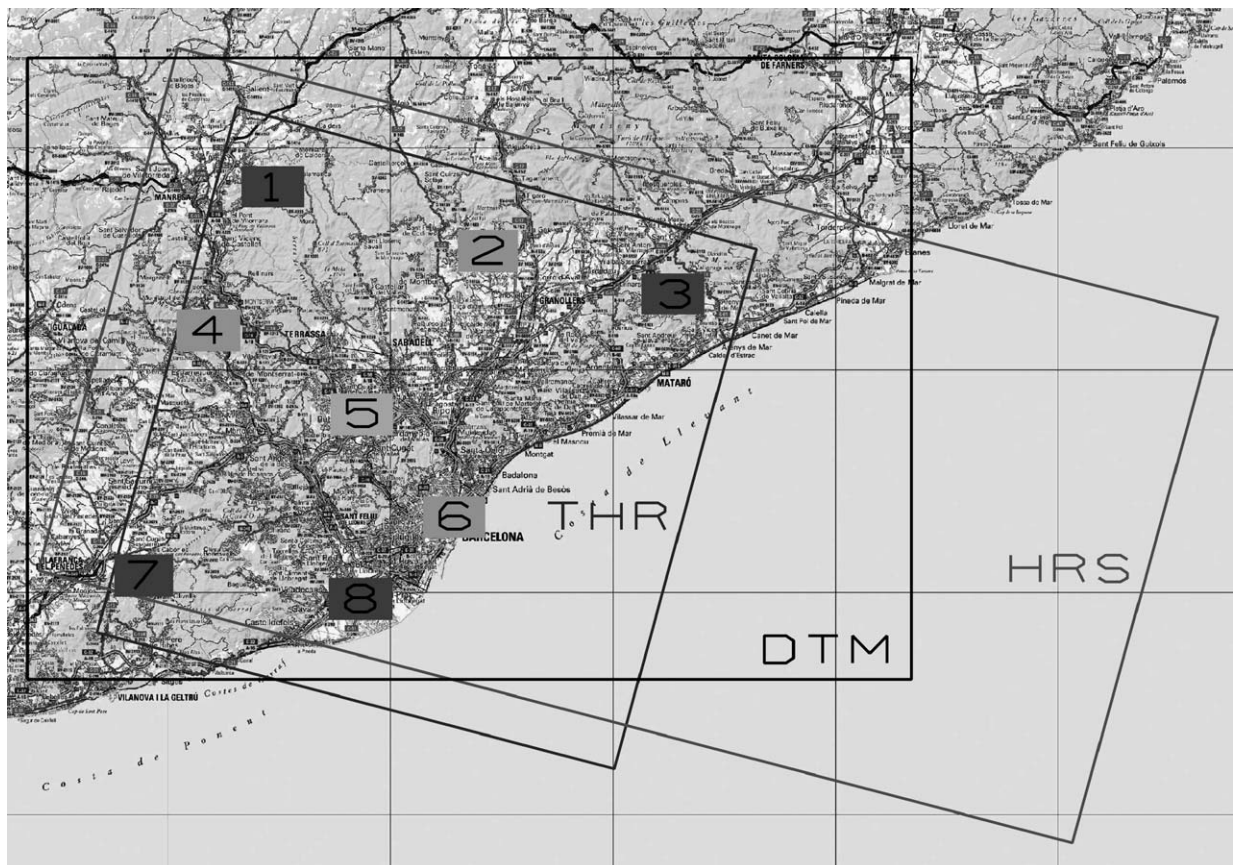4. Bundle adjustment to estimate the correction polynomials

Fig. 1. Location of the reference DTM (DTM rectangle) and the 8 test sites.
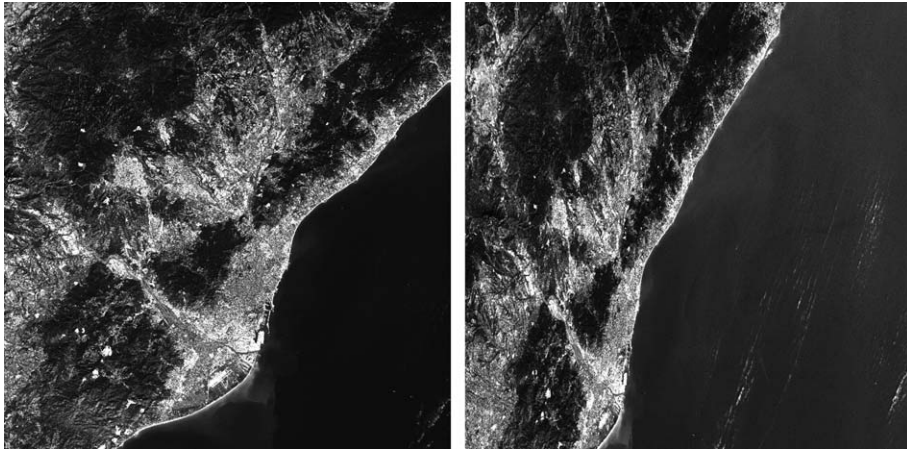
Fig. 2. HRG image (left, GSD: 2.5×2.5 m) and HRS1 image (right, GSD: 10×5 m).

5. Transformation of image mass points into object space
6. Results: Accuracy assessment of object points
7. Results: Accuracy assessment of generated DEM.

3.1. Direct geo-referencing

As a first step, the images are directly geo-referenced applying the model described in the SPOT Satellite Geometry Handbook (SPOT Image, 2002) using the supplied orientation parameters and look angles. The comparison between directly geo-referenced points and the orthoimages shows that the supplied orientation parameters provide a horizontal accuracy better than 30 m.

3.2. Measurement of control and check points

In each test site 5 points are measured on a digital photogrammetric workstation with matching support in the HRS and HRG images and also in the corresponding orthoimage. For a better point identification the different image scales of the HRS images are adapted applying a scale factor of 2 in scan direction. Nevertheless, the point identification is very difficult, even by an experienced operator, especially in the scaled oblique looking HRS images. Only points lying on the ground are useful because the reference heights are taken from a terrain model. Due to the presence of forests and buildings in wide areas of test sites #3, #4 and #6 it was not possible to measure all 5 points. Altogether, 19 points in test sites #1, #3, #7 and #8 are defined as control points and 17 points of test sites #2, #4, #5 and #6 as check points (see Fig. 3).

3.3. Mass point generation in image space

For the mass point generation in image space a modified region growing algorithm, originally developed by (Otto and Chau, 1989), is used, which already had successfully been applied to SPOT-1 images in the early 1990s (Heipke and Kornus, 1991). Starting from a couple of manually measured so-called seed points, the algorithm matches the four neighbour pixels (left, right, upper and lower) at a given distance. For this study 1 pixel distance of the original HRS image is chosen. If the matching result meets some specified criteria (a minimum correlation coefficient, a maximum number of iterations, etc.) the point is added to a list and serves itself as a new seed point. The process ends after all points of the list are matched and there are no more neighbours meeting the criteria.

The algorithm is applied to sections within the 8 test sites of the HRS1, HRS2 and the HRG images with a size of approx. 2700×3300 HRG pixels. Previously the HRS images have been adapted to the HRG resolution applying a scale factor 2 in flight direction and a scale factor 4 in scan direction. For each test site, 3 matching combinations are calculated: (a) HRG–HRS1, (b) HRG–HRS2 and (c) HRS2–HRS1. The HRG-points successfully matched in combination (a) are entered into the matching combination (b) as, so-called, transfer points, i.e. only the coordinates in the second image of the combination are determined while the coordinates in the first image resulting from the previous matching run are kept. Accordingly, the resulting HRS2-points of the second combination again form the transfer points of combination (c).

The points obtained from the 3 matching runs are classified into 3 groups depending on the number of
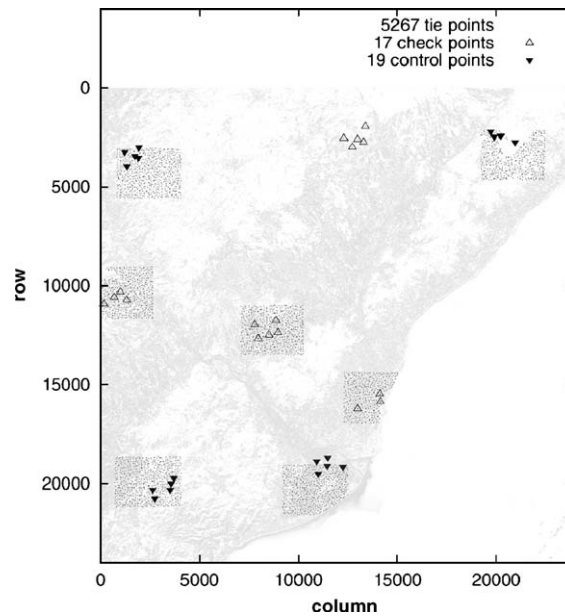
Fig. 3. Location of control, check and tie points in the HRG image.

combinations they have successfully been matched. Group 1 contains pure two-ray-points, which are matched in only one of the combinations HRG–HRS1 or HRG–HRS2. Group 2 contains three-ray-points, which are matched in 2 combinations (HRG–HRS1 and HRG–HRS2 or HRG–HRS2 and HRS2–HRS1). Group 3 contains redundant three-ray-points, which are matched in all 3 combinations. The HRS1 coordinates result from two different combinations of matching runs (HRG–HRS1 and HRS2–HRS1) and are averaged. The deviations from the average ΔX^{S1} and ΔY^{S1} are used to calculate standard deviations $\sigma_{\Delta X}^{S1}$, $\sigma_{\Delta Y}^{S1}$ as a further quality criterion. In the following DEM generation only 3-ray points with a correlation coefficient ρ higher than 0.7 are considered. For point group 3 additionally small deviations are required. The applied criteria is $\Delta X^{S1} < 3$ $\sigma_{\Delta X}^{S1}$ and $\Delta Y^{S1} < 3$ $\sigma_{\Delta Y}^{S1}$. Table 1 shows the obtained point numbers in the different point groups for all 8 test sites. The big majority of the points could be matched in all 3

images. Most of them belong to point group 3 and also meet the defined criteria. This demonstrates that the applied matching algorithm is suitable to produce a reliable and sufficiently dense point cloud.

From point group 3 also a subset of points is selected as input for the bundle adjustment using a regular grid of 100×100 pixel mesh size. Taking the point with the maximum correlation coefficient within a grid mesh, 5267 regularly distributed tie points are obtained in 7 test sites (see Fig. 3). From test site #2 no tie points were extracted at all in order to be used as a pure check site.

3.4. Bundle adjustment

In order to compensate for possible systematic errors in either the exterior orientation or the interior orientation data (look angles) of SPOT-5 a new functional model was implemented into ICC's adjustment software GeoTeX (Colomina et al., 1992), which is

Table 1
Results of region growing image matching

Test site	#1	#2	#3	#4	#5	#6	#7	#8
Two-ray-points	75,643	152,505	71,656	79,575	119,694	72,379	54,551	100,055
Two-ray-points with $\rho > 0.7$	39,108	134,013	29,233	57,965	103,744	49,391	41,459	88,808
Three-ray-points matched in 2 combinations	166,657	205,687	177,825	170,871	109,805	136,127	143,485	137,034
Three-ray-points in 2 combinations with $\rho > 0.7$	85,497	164,198	58,468	113,097	87,566	95,301	82,035	117,369
Points matched in 3 combinations	728,825	678,645	467,015	596,486	768,396	541,319	797,748	686,262
Points in 3 combinations with $\Delta^{S1} < 3\sigma_\Delta^{S1}$	595,051	601,042	393,743	485,450	678,165	454,615	697,439	595,961
Three-ray-points selected for DEM generation	680,548	765,240	452,211	598,547	765,731	549,916	779,474	713,330

described in the following. It applies global correction terms to the given position and attitude of the common trajectory and individual correction terms to the look angles of each single sensor. Third degree polynomials are applied as correction functions.

3.4.1. Functional model

The functional model is based on Eq. (1), which relates the look direction vector $\boldsymbol{u}_1$ in the navigation reference coordinate system to the look direction in the terrestrial coordinate system, defined by the difference between the point vector $[X, Y, Z]^T$ and the projection centre $[X_0, Y_0, Z_0]^T$.

$$\boldsymbol{u}_1 = \begin{bmatrix} -\tan(\Psi_Y)_p^S \\ \tan(\Psi_X)_p^S \\ -1 \end{bmatrix} = \frac{1}{\mu} R_{21}^{-1} \cdot R_{32}^{-1} \cdot \begin{bmatrix} X-X_0 \\ Y-Y_0 \\ Z-Z_0 \end{bmatrix} \quad (1)$$

where

$\boldsymbol{u}_1$ defines the look direction vector in the navigation reference coordinate system. It depends on the look angles $(\Psi_X)_p^S$ and $(\Psi_Y)_p^S$, which are given for each pixel p of the sensor line S.

R_{21} is the rotation from the navigation reference coordinate system to the orbital coordinate system. It depends on the interpolated roll, pitch and yaw attitude angles $a_r(t)$, $a_p(t)$, $a_y(t)$, which are given as a time series at 8 Hz frequency.

R_{32} is the rotation from the orbital coordinate system to the terrestrial coordinate system. It depends on the centre of mass position $P(t)$ of the satellite and the velocity vector $V(t)$, which are given as time series at a 30 s time interval.

Eliminating the scale factor μ the applied pseudo-observation Eq. (2) are obtained:

$$0 = \frac{r_{11}(X-X_0) + r_{12}(Y-Y_0) + r_{13}(Z-Z_0)}{r_{31}(X-X_0) + r_{32}(Y-Y_0) + r_{33}(Z-Z_0)} - \tan(\Psi_Y)_p^S$$

$$0 = \frac{r_{21}(X-X_0) + r_{22}(Y-Y_0) + r_{23}(Z-Z_0)}{r_{31}(X-X_0) + r_{32}(Y-Y_0) + r_{33}(Z-Z_0)} + \tan(\Psi_X)_p^S \quad (2)$$

where $r_{i,j}$ are the components of $R = R_{21}^{-1} R_{32}^{-1}$.

The coefficients of the correction polynomials are the actual unknowns of the adjustment, which are applied to the parameters of the external orientation E_t, i.e. to the position vector $\boldsymbol{P}(t) = [X_0, Y_0, Z_0]^T$ and to the attitude angles $a_r(t)$, $a_p(t)$, $a_y(t)$ as well as to the parameters of the internal orientation I_p^S, i.e. to the look angles $(\Psi_X)_p^S$ and $(\Psi_Y)_p^S$ of sensor line S and pixel p.

$$E(t) = E_t + A_E + B_E(t-t_c) + C_E(t-t_c)^2 + D_E(t-t_c)^3 \quad (3)$$

$$I^S(p) = I_p^S + A_I^S + B_I^S\left(\frac{p-p_c}{1000}\right) + C_I^S\left(\frac{p-p_c}{1000}\right)^2 + D_I^S\left(\frac{p-p_c}{1000}\right)^3 \quad (4)$$

The external orientation parameters $E(t)$ (Eq. (3)) enter in Eq. (2). They are derived from the interpolated parameter E_t at time t of the corresponding image line and the 3rd order correction polynomial with its unknown coefficients A_E, B_E, C_E and D_E. t_C here is defined as the epoch of the central line (#12001) of the HRG image. The internal orientation parameters $I^S(t)$ (Eq. (4)) also enter into Eq. (2). They are derived from the parameter I_p^S of the interpolated sensor position p and the 3rd order correction polynomial with its unknown coefficients A_I^S, B_I^S, C_I^S and D_I^S. p_C here is defined as the central pixel of the respective sensor line S.

This model involves 48 unknowns when 3 viewing directions are involved (like in this evaluation: HRS1, HRS2 and HRG), i.e. 4 unknowns for each of the 6 external orientation parameters and 2 times 4 unknowns for each of the 3 sensor lines. In practice, only a subset of these 48 unknowns will be significantly determinable and the rest of the parameters need to be fixed in order to avoid over-parameterization problems.

3.4.2. Input

The following observations are introduced into the adjustment:

- Image coordinates of 19 control and 17 check points with an a priori standard deviation σ of 0.5 pixel, measured in the HRS1, HRS2 and the HRG images (see Fig. 3),
- image coordinates of 5270 tie points, obtained by automated image matching in the HRS1, HRS2 and the HRG images ($\sigma = 0.5$ pixel, see Fig. 3),
- horizontal object coordinates of 19 control points ($\sigma = 2.5$ m, corresponding to the ground sampling distance of the HRG-channel, which is limiting the point identification accuracy),
- heights of 19 control points ($\sigma = 2.2$ m $= 2 \sigma_{DTM}$).

The supplied look angles, ephemeris, velocity and attitude parameters enter as constants in the adjustment.

Table 2
Estimated CPC (x) for look angles, standard deviations (σ_x), significance (x/σ_x) and maximum effect (E) [pixel]

Channel		A_x	B_x	C_x	D_x	A_y	B_y	C_y	D_y
HRG	x	5.3E-06	1.0E-06	–	–	2.8E-05	–	–	–
	σ_x	7.8E-06	1.1E-07	–	–	3.3E-06	–	–	–
	x/σ_x	0.7	9.9	–	–	8.6	–	–	–
	E	1.8	4.2	–	–	9.5	–	–	–
HRS1	x	−4.9E-06	–	–	–	1.5E-05	–	−4.2E-07	−6.9E-08
	σ_x	1.3E-05	–	–	–	5.6E-06	–	4.7E-07	9.1E-08
	x/σ_x	0.4	–	–	–	2.6	–	0.9	0.8
	E	−0.4	–	–	–	2.4	–	−2.6	−2.5
HRS2	x	–	–	–	–	–	–	−4.6E-07	−7.4E-08
	σ_x	–	–	–	–	–	–	4.8E-07	9.6E-08
	x/σ_x	–	–	–	–	–	–	1.0	0.8
	E	–	–	–	–	–	–	−2.8	−2.6

A_x–D_x apply in scan direction, A_y–D_y in flight direction.

3.4.3. Results

In order to minimize correlation effects between external and internal orientation, the 24 correction polynomial coefficients (CPC) for the external orientation parameters were fixed in a first step and only 24 CPC for the look angles were estimated. Later in a second step, i.e. after the set of significantly determinable CPC (for the look angles) has been found, this set is fixed and the 24 CPC for the external orientation parameters are estimated.

3.4.3.1. Bundle adjustment using HRS and HRG data.
In a series of adjustment runs those CPC, whose estimated values are small compared to their estimated standard deviations are consecutively fixed to zero. Simultaneously, it is monitored whether the fixing of the CPC provokes a systematic alignment or an increase of the residual vectors of the control points in image or in object space. In this case the CPC are not fixed, even if the relation between its value and their standard deviation is small. After a series of adjustment runs it turned out, that 15 of the 24 CPC can be fixed and consequently 9 CPC are determined at an acceptance level of significance. In Table 2, their estimated values (x), the estimated standard deviations (σ_x), their significance (x/σ_x) and the maximum effect (E) in pixel at the edges of the CCD-array are listed. The most

significantly estimated CPC are B_x and A_y of the HRG channel. B_x can be interpreted as a slight change of the scale in scan direction. The maximum effect at the sensor edge is 4.2 pixels, which corresponds to approximately 1 pixel of the HRS channels. A_y indicates a displacement of the HRG sensor in flight direction of 9.5 pixels. The other 7 CPC are determined less significantly with a maximum effect of less than 3 pixels.

Table 3 shows the statistics on the differences of the coordinates at the 17 check points, indicating an empirical accuracy of approximately 2 m in Easting (dE), Northing (dN) and Height (dH) after applying the significant CPC. Compared to the HRS ground sampling distance (5×10 m) these 2 m are very close to the point identification accuracy, which usually is 0.2–0.3 pixel. This demonstrates that the SPOT-5 imaging geometry is properly modelled by the presented approach.

Table 4 reports the statistical analysis of the differences between the 5235 estimated tie point heights and their interpolated DTM heights. Here the standard deviation is considerably worse since many of the automatically matched points lie on top of vegetation or artificial objects, which are not represented in the reference DTM. This error is reflected in the mean height difference value of 2.1 m and also, in the respective histogram, showing higher frequencies for positive height differences (see Fig. 4). These points

Table 3
Statistics on coordinate differences dE, dN, dh [m] of the 17 check points

	HRS and HRG data					HRS data only				
	Min	Mean	Max	RMS	σ	Min	Mean	Max	RMS	σ
dE	−4.4	−2.1	1.4	2.7	1.7	−5.0	−1.7	6.1	3.82	3.5
dN	−6.1	0.8	3.7	2.3	2.2	−5.0	0.5	5.1	2.92	3.0
dH	−4.4	0.2	2.5	1.9	1.9	−2.8	1.0	4.2	2.08	1.9

Table 4
Statistics on height differences dh [m] between 5235 tie points and the reference DTM

	HRS and HRG data					HRS data only				
	Min	Mean	Max	RMS	σ	Min	Mean	Max	RMS	σ
dH	−22.2	2.1	63.3	6.1	5.7	−22.1	2.6	60.3	6.6	6.0

must actually be compared to a digital surface model, which was not available in this study.

The second adjustment step employing CPC for the position and attitude parameters (and keeping fixed the estimated set of CPC for the look angles) did not show a significant improvement. Thus, it is not necessary to apply corrections to the attitude and position parameters.

3.4.3.2. Bundle adjustment using HRS data only.

Since HRS/HRG imagery is not always available an additional adjustment is done considering pure SPOT-5 HRS data. It turned out, that without HRG data none of the CPC can be determined significantly. This is not surprising, since the effect of the estimated CPC for the HRS1 and HRS2 channels proved to be very small (less than 3 pixels maximum, see Table 2). Consequently, an adjustment with all CPC fixed to zero was calculated. The obtained results are listed on the right half of Tables 3 and 4. They show, that without the nadir viewing channel the height accuracies of both the check points (see Table 3) and the tie points (see Table 4) remain more or less unchanged, while the horizontal accuracy at the checkpoints decreases. This is in accordance to former experiences with the German MOMS-02 camera, which already turned out, that the presence of a nadir view only improves the horizontal accuracy and does not geometrically contribute to a better height accuracy (Ebner et al., 1992).

3.5. Transformation of image mass points into object space

After the adjustment the image points can rigorously be transferred into object space using the estimated interior and exterior orientation parameters. From the resulting 3D mass point cloud Triangular Irregular Network (TIN) models are produced, which later are converted into 10 m grid step DEM.

3.5.1. Rigorous model

First, the image points are transformed point-wise by a local adjustment based on Eq. (5), which is derived from the inverted Eq. (1) using the rigorous model and the estimated parameters listed in Table 2. Three equations are defined for each point and image:

$$\begin{bmatrix} X \\ Y \\ Z \end{bmatrix} = \begin{bmatrix} X_0 \\ Y_0 \\ Z_0 \end{bmatrix} + \mu \cdot R_{32} \cdot R_{21} \cdot u_1 \qquad (5)$$

Thus, in the case of three-ray-points 9 equations are formulated to solve for 6 unknowns (X, Y, Z, μ_1, μ_2, μ_3). In the case of two-ray-points, there are 6 equations to
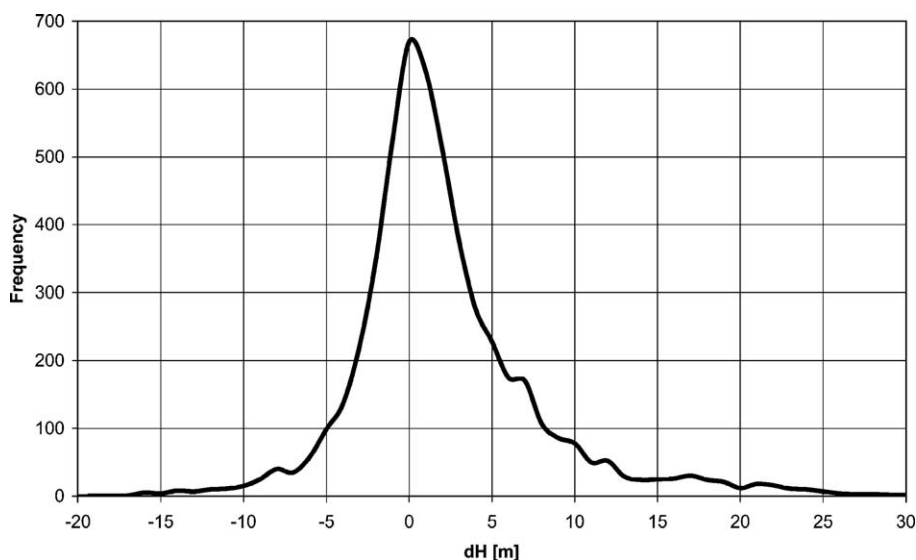

Fig. 4. Histogram of height differences between tie points and the reference DTM.

solve for 5 unknowns (X, Y, Z, μ_1, μ_2). The transformation is applied for the image mass points of test sites #2, #4, #5 and #6 separately for the 3 point groups (see Section 3.3). The test sites containing control points (#1, #3, #7 and #8) are not included in the accuracy analysis.

3.5.2. Rational functions

In a second approach rational functions are applied derived from point cubes of 1331 equally distributed points. The cube has a grid step of 1200 pixels in columns and rows (2400 in the case of the HRG image) and 250 m grid step in object space height (from −250 to 2250 m). The X,Y object coordinates are calculated for the respective image column, image row and object height, once for the HRS/HRG data applying the 9 estimated correction parameters (see Section 3.4.3.1) and a second time for the pure HRS data without applying correction polynomials (see Section 3.4.3.2). From the two point cubes two sets of best estimated rational functions coefficients are determined by least squares adjustment. For forward and backward looking directions rational functions of degree 3 in numerator and denominator are used. In case of the nadir looking direction a 3rd degree polynomial is adjusted, since it has not been possible to adjust any polynomial denominator without zeros in the domain of the image footprint. With these results the image mass points of test sites #2, #4 and #5 are transformed again into object space. The statistics on the height differences between the resulting object coordinates and the coordinates computed with the rigorous model turned out to be negligible (see Table 5). Under the conditions of this data set with a smooth movement of the satellite it seems that stereoplotting with rational functions is as accurate as using a rigorous model. This agrees with the results obtained by (Alamús et al., 2000) and (Ebner et al., 1992) with other satellites. Therefore, no new DEM are produced, i.e. it is assumed, that this rational function approach is also represented by the strict model.

3.6. Results: accuracy assessment of object point heights

The resulting object point heights are compared to the reference DTM and analyzed. The differences give more reliable indications about the geometric SPOT-5 accuracy potential than the final DEM accuracy does, which additionally includes the DEM interpolation error. Fig. 5 shows these height differences dh after the rigorous transformation of the image mass points for test site #5 in a colour coded representation. In most parts of the image the matching algorithm has worked quite well, while small black areas indicate where the image matching was not successful, causing gaps in the 3D point cloud and, consequently, in the DEM. The corresponding orthoimage in Fig. 6 identifies these gaps as areas with low contrast (like the wide road in the bottom centre) or homogeneous texture (like the forest in the upper right corner of the image). It can also be seen, that red points, indicating height differences bigger than 5 m, mainly appear in the urban area on the left or in forest zones, e.g. on the upper right. This illustrates quite well the difference between the produced point cloud, representing the visible surface, and the reference terrain model, representing the bare Earth's surface.

Table 6 shows the statistics of the comparison between the point heights and the reference DTM. Again, the results represent the complete unfiltered sets of fully automatically matched points, which include blunders and points on top of vegetation and buildings. For that reason the RMS values must be interpreted as very conservative, i.e. they would be considerably better if only ground points would be taken into account or a high quality surface model had been available as a reference. Since test site #6 covers the Barcelona urban area and contains only few ground points, the accuracy potential of SPOT-5 should rather be deduced from the results of the other test sites #2, #4 and #5. The points matched in 3 combinations yield, as expected, the best results with RMS height differences of about 4 m in the moderate terrain of the test sites #2 and #5 and of about 5 m in the mountainous terrain of test site #4. There also exist some blunders with differences up to nearly 90 m. Three-ray-points matched in 2 combinations lead to acceptable 4–5 m height differences in moderate terrain. In mountainous terrain, however, the RMS differences increase to nearly 12 m. For two-ray-points this situation is even worse. In Fig. 7 the histograms of the height

Table 5
Statistics on height differences dh [m] between the points, matched in 3 combinations, derived from rational functions and from the strict model

Test site	N	Min	Mean	Max	RMS	σ
#2	601,041	−9.3	−0.6	15.7	0.6	0.2
#4	485,449	−16.6	−0.3	18.1	0.5	0.3
#5	678,164	−8.5	−0.4	14.8	0.5	0.2

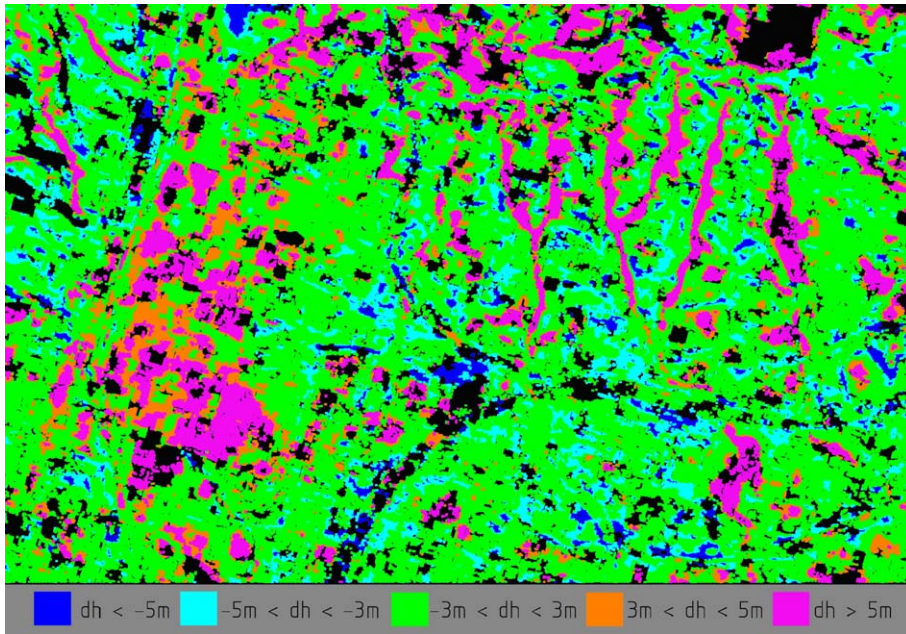Fig. 5. Color coded height differences between points and reference DTM for test site #5 (section: 5.3 × 3.6 km).

differences for the 3 point groups are depicted for test site #5.

Table 7 shows the respective statistics on height differences obtained from a pure HRS data set without considering the HRG data. This implies new matching runs with two-ray-points only. Since the bundle adjustment did not yield significant results (see Section 3.4.3.2), the matched image points are directly transferred into object space using the supplied orientation data and the local adjustment described in Section 3.5.1. The standard deviations are approximately 20% worse compared to the results achieved with bundle adjustment and matching in 3 combinations (see Table 6).

It was stated above, that the nadir looking view of the HRG camera does not contribute very much to the

Fig. 6. Orthoimage of test site #5 (section: 5.3 × 3.6 km).

Table 6
Statistics on height differences d*h* [m] between the 3D object points and the reference DTM

Test site	N	Min	Mean	Max	RMS	σ
Point group 3: three-ray-points from 3 matching runs						
#2	601,042	−27.5	0.3	30.2	3.8	3.8
#4	485,450	−85.5	0.3	88.0	5.2	5.1
#5	678,165	−49.4	1.5	33.5	4.0	3.7
#6	446,380	−39.7	10.9	66.9	13.0	7.2
Point group 2: three-ray-points from 2 matching runs						
#2	164,411	−69.1	0.1	56.3	4.1	4.0
#4	119,301	−142.2	1.6	165.4	11.6	11.4
#5	86,635	−109.0	1.1	99.0	5.1	5.0
#6	68,979	−106.7	8.1	95.9	12.4	9.4
Point group 1: two-ray-points						
#2	134,013	−175.3	0.1	99.8	5.4	5.4
#4	57,965	−141.1	1.7	203.6	13.8	13.7
#5	103,744	−223.6	1.3	226.3	6.0	5.9
#6	35,571	−151.6	6.6	151.9	12.4	10.6

height accuracy. This is true from the geometric point of view in the case of well identifiable check points. Here, in the automatic mass point generation process by image matching, we see that the third view considerably improves the results in terms of accuracy and reliability, especially in mountainous regions.

3.7. Results: assessment of DEM accuracy

The DEM accuracy is assessed with respect to the terrain type (flat/moderate, mountainous), the number of SPOT-5 viewing directions (HRS/HRG: 3, HRS: 2) and the DEM generation method (matching in image space using region growing, matching in object space using the commercial ISAE software).

3.7.1. Matching in image space
After the image point cloud is rigorously transformed to object space (as described above), 10 m grid step DEMs are interpolated within the areas of test sites #2, #4 and #5. The left part of Fig. 8 shows the standard deviations obtained from the height differences between the DEM raster points and the reference DTM in moderate/flat areas (test sites #2 and #5) and in mountainous areas (test site #4). The achieved DEM accuracy in moderate/flat terrain using all three viewing directions is with 4.4 m far better than the HRS pixel footprint (5×10 m). This is an impressively good result considering the presence of points on top of vegetation and buildings. Without HRG data the accuracy deteriorates about 10% in the moderate/flat terrain and about 60% in the mountainous area. The deterioration is mainly caused by occlusion because in steep terrain the valleys are only seen by one of the two stereo views and therefore are not well represented in the DEM. This underlines again the importance of the third (nadir) view in mountainous terrain.
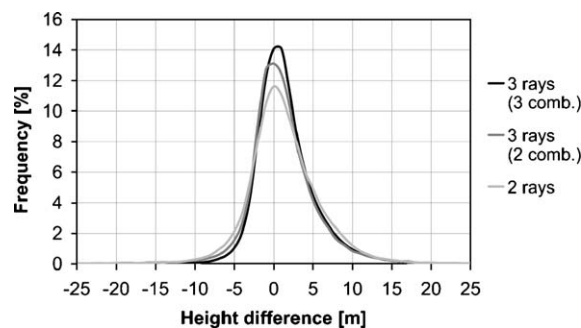

Fig. 7. Histogram of height differences d*h* [m] for test site #5.

Table 7
Statistics on height differences dh [m] between the 3D object points derived from HRS data only and the reference DTM

Test site	N	Min	Mean	Max	RMS	σ
#2	997,949	−63.4	8.6	121.2	9.8	4.7
#4	940,159	−155.1	9.1	288.3	14.0	10.7
#5	956,022	−100.5	9.6	75.9	10.6	4.6
#6	575,775	−131.7	18.6	154.1	21.1	9.9

3.7.2. Matching in object space (ISAE)

A further set of DEMs is produced using the commercial software ISAE (Krzystek, 1991), which applies feature based matching in object space. The major advantage is its operational environment, compared to the more scientific approach described so far. Once the rational functions are computed the program can be run by operators and does not need the interaction of experts, which is of high importance if a large amount of SPOT scenes are to be processed on a routine basis. For the DEM generation the already calculated two sets of rational functions are applied, which were derived from HRS/HRG data and from pure HRS data (see Section 3.5.2). The grid step is set to 45 m in order to ensure sufficient reliability in the DEM generation process (a minimum average of 5 points per grid mesh). For both data sets more than 17 millions of matching points are found, which fulfil this requirement. Fig. 9 shows the resulting DEM in a grey value coded representation, which covers the entire HRS image scene. An internal height accuracy of 0.9 m is obtained for the first DEM (HRS/HRG) and 1.3 m for the second (HRS), which proved to be too optimistic compared to the empiric quality measures. For the entire DEM a standard deviation of 8.3 m is achieved applying the rational functions from HRS/HRG data. From pure HRS data 9.2 m are obtained. The right part of Fig. 8 reflects the accuracy in the moderate/flat and mountainous test site areas. It is about 20–25% worse compared to the results obtained by matching in image space, which is at least partly due to the bigger grid spacing.

Summarizing the results, which are graphically represented in Fig. 8, three simple statements can be made:

1. The DEM accuracy in mountainous terrain is lower than in moderate and flat terrain, which is obviously due to the higher probability of occlusions and due to the higher impact of horizontal errors. In addition, homogenous image patterns, e.g. in forest areas, which also obstruct the matching process, produce gaps in the point cloud and later in the DEM. Here is the biggest potential of accuracy improvement by manual interaction.
2. Three viewing directions (HRS/HRG) are better than two (HRS only). Although the nadir viewing camera HRG does not geometrically contribute to a better height accuracy, its presence supports the accuracy and reliability of the matching process, especially in mountainous regions, where it also helps to bridge
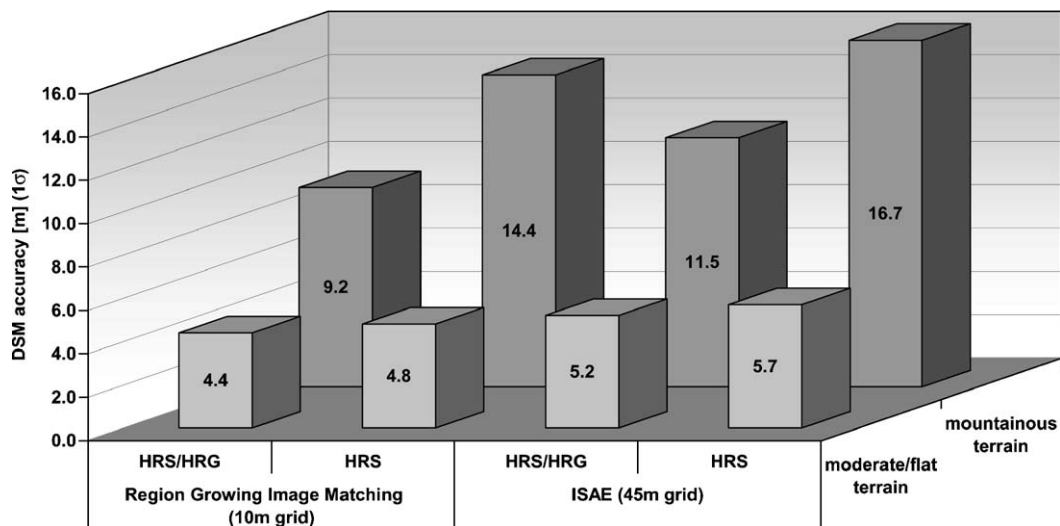

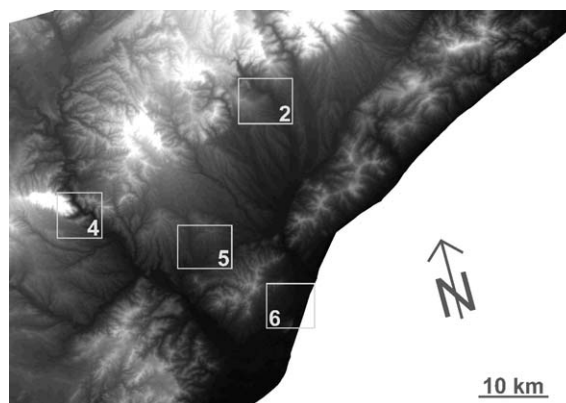Fig. 8. Standard deviations of height differences between the produced DEM and the reference DTM.

Fig. 9. Grey value coded DEM representation of the entire image scene (approx. 80×60 km) generated by ISAE using the HRS1 and HRS2 images at 45 m grid size. The location of the four check areas is marked by light grey rectangles.

occlusions. Nevertheless, HRG imagery, if available at all, does not cover the whole HRS scene and therefore it is not always possible to use a three viewing (HRS/HRG) approach.

3. DEMs generated with region growing image matching are more accurate than the ISAE-DEM, which probably is at least partly caused by the different grid spacing. The actual reasons have not been analysed in this study.

4. Conclusions

This report describes the DEM generation using SPOT-5 HRS and HRG images. Correction polynomials for the provided look angle values of each camera (interior orientation) are estimated by bundle block adjustment using 19 ground control points in 4 control areas located in the corners of the covered terrain. The application of correction polynomials for position and attitude (exterior orientation) proves to be not necessary. The bundle adjustment results in a point accuracy of 2 m in Easting, Northing and Height, which is demonstrated by 17 independent check points, distributed in 4 check areas.

An automated region growing image matching algorithm is applied to generate mass points in image space, which later are transformed into object space using a rigorous model and also rational functions. Without manual editing and/or filtering of the resulting point cloud an RMS height error of approximately 4 m (5 m in mountainous terrain) is obtained for three-ray-points matched in 3 combinations (nadir–backward, nadir–forward, backward–forward). For three-ray-points matched in 2 combinations and for two-ray-points the RMS error is worse especially in mountainous areas. It turns out, that the point cloud from the applied matching process can be produced automatically with

sufficient density in wide parts, but not in all parts of the images. The algorithm fails in areas with poor image contrast or homogenous texture like forests, broad streets, large agricultural areas, etc. The presented results reflect the accuracy potential of SPOT-5 HRS, which can be achieved by largely automatic processing; i.e., it still bears a considerable potential of improvement, which depends on the amount of manual editing and appropriate filtering in order to fill the gaps in the automatically generated point cloud and to exclude blunders and points on top of vegetation and artificial objects. Nevertheless, it has been demonstrated that even under these conditions DEM production with SPOT-5 data in flat and moderate terrain is possible with an absolute accuracy better than 5 m and up to 9 m in mountainous areas.

References

Alamús, R., Kresse, W., Langner, M., 2000. Accuracy potential of point measurements in MOMS-images using a rigorous model and a rational function. International Archives of Photogrammetry,

Remote Sensing and Spatial Information Sciences 33 (Part B4), 515–517 (Amsterdam, The Netherlands).

Baudoin, A., Schroeder, M., Valorge, C., Bernard, M., Rudowski, V., 2004. The HRS-SAP initiative: a scientific assessment of the High Resolution Stereoscopic instrument on board of SPOT-5 by ISPRS investigators. International Archives of Photogrammetry, Remote Sensing and Spatial Information Sciences 35 (Part B1), 372–377 (Istanbul, Turkey).

Bouillon, A., Bernard, M., Gigord, P., Orsonia, A, Rudowski, V, Baudoin, A., 2006-this issue. SPOT-5 HRS Geometric Performances: Using Block Adjustment as key issue to improve quality of DEM generation. ISPRS Journal of Photogrammetry and Remote Sensing 60, 134–146. doi:10.1016/j.isprsjprs.2006.03.002.

Colomina, I., Navarro, J., Térmens, A., 1992. GeoTeX: a general point determination system. International Archives of Photogrammetry and Remote Sensing 29 (Part B3), 656–664 (Washington D.C, USA).

Ebner, H., Kornus, W., Ohlhof, T., 1992. A simulation study on point determination for the MOMS-02/D2 space project using an extended functional model. International Archives of Photogrammetry and Remote Sensing 29 (Part B4), 458–464 (Washington D.C., USA).

Heipke, C., Kornus, W., 1991. Nonsemantic photogrammetric processing of digital imagery — the example of SPOT stereo scenes. In: Ebner, Fritsch, Heipke (Eds.), Digital Photogrammetric Systems. Wichmann Verlag Karlsruhe, Germany. ISBN: 3-87907-234-5, pp. 86–102.

Krzystek, P., 1991. Fully automatic measurement of digital elevation models. Proceedings of the 43rd Photogrammetric Week, Stuttgart, pp. 203–214.

Otto, G., Chau, T., 1989. Region growing algorithm for matching of terrain images. Image and Vision Computing 2 (7), 83–94.

SPOT Image, 2002. SPOT Satellite Geometry Handbook, S-NT-73_12-SI, Edition 1, Revision 0, 15. 01. 2002.

SPOT Magazine No. 31, 2000. The secrets of SPOT-5 Supermode, Sept. 2000.